Nanotechnology **21** (2010) 065708 (7pp) doi:10.1088/0957-4484/21/6/065708

# The use of microwave plasma-assisted CVD on nanostructured iron catalysts to grow isolated bundles of carbon nanotubes

**M B Assouar[1], M Dossot[2], S Rizk[1], C Tiusan[1] and J Bougdira[1]**

[1] Institut Jean Lamour, Nancy University—CNRS, Boulevard des Aiguillettes, BP 239, F-54506 Vandoeuvre-lès-Nancy Cédex, France
[2] Laboratoire de Chimie Physique et Microbiologie pour l'Environnement, Nancy University—CNRS, 405 rue de Vandoeuvre, F-54600 Villers lès Nancy, France

E-mail: Badreddine.Assouar@lpmi.uhp-nancy.fr

Received 13 October 2009, in final form 9 December 2009
Published 8 January 2010
Online at stacks.iop.org/Nano/21/065708

**Abstract**
Catalysts play a key role in the growth of carbon nanotubes. The microwave plasma-assisted chemical vapor deposition (MPACVD) method is now commonly used for directional and conformal growth of carbon nanotubes (CNTs) on substrates. In this work, we report on the effect of $H_2$ plasma pre-treatment on the diameter and density of iron catalyst nanoparticles for different iron layer thicknesses in order to grow isolated bundles of CNTs. Atomic force microscopy shows first that as plasma power density increases, iron nanoparticle diameters decrease, which is due to the increasing of gas dissociation giving more ion bombardment energy, and second that the diameter of nanoparticles decreases with the catalyst thickness. The growth of CNT was carried out under different $CH_4$ concentrations for different iron film thicknesses. Transmission electron microscopy and Raman spectroscopy show that the synthesized CNT were of good quality and had an outer diameter between 5 and 10 nm.

(Some figures in this article are in colour only in the electronic version)

## 1. Introduction

In recent years, we have noted many significant developments around different types of carbon structures such as diamond, diamond-like carbon (DLC) thin films, nanoclusters, bucky balls or fullerenes, and carbon nanotubes (CNTs). While there are many potential industrial applications for diamonds, DLCs (carbon nanostructures like nanodiamonds and carbon nanotubes) are expected to find applications in numerous fields, as presented recently by Melechko *et al* [1]. Martel *et al* [2] have shown some results on field effect transistors based on single or multiwall nanotubes. Gröning *et al* [3] published a review paper demonstrating that CNTs can be clearly considered as the materials taking us from nanoscience to nanotechnology in the field of electron emission technology. Another application, which is interesting due to the biocompatibility of the CNTs, is using them as electrochemical biosensors [4], or as gas sensors [5].

The most common technique for depositing such carbon nanotubes is generally a suitable chemical vapor deposition (CVD) process or an arc discharge process. Meyappan *et al* [6] reported on the importance of plasma-assisted chemical vapor deposition (PACVD) techniques in the production of CNTs. The review paper from Melechko *et al* [1] presents the state of the art in vertically aligned carbon nanofibers and carbon nanostructured materials produced in PACVD reactors, and their functionalization. Minea *et al* [7] adopted yet another PACVD technique to obtain CNTs. Their technique, based on the electron cyclotron resonance production of plasma, produces carbon nanofibers at relatively low temperatures, from 400 °C to room temperature. The advantage is that plasma reactive species can be created even at room temperature, allowing for a large possibility of applications in the future. In general, decoupling the plasma generation and reactive species generated during the deposition processes can be done by a remote pulsed microwave plasma-assisted chemical vapor deposition (MPACVD) system. The difference between these two techniques is that the first is able to independently control the plasma density as well as the degree of dissociation, while the second controls the surface

 

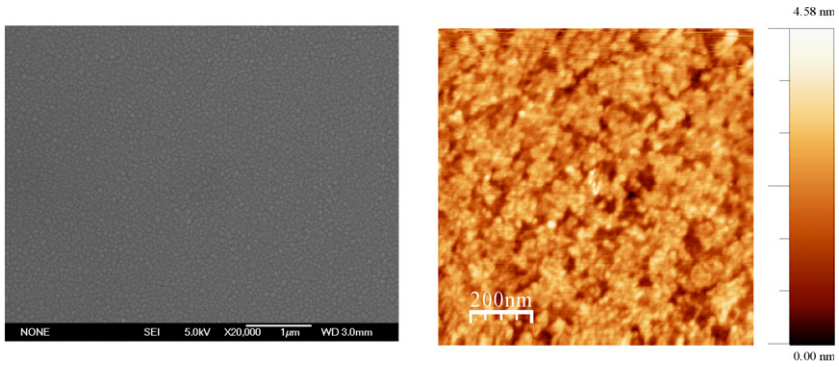


**Figure 1.** SEM and AFM micrographs of an as-deposited 10 nm catalyst iron film.

chemistry and the growth mechanisms. In this study, we have developed an MPACVD system using a continuous microwave source at 2.45 GHz and have obtained interesting results for diamond growth, especially by studying the role of atomic hydrogen in such a process [8–10].

Before the CNT growth, the catalyst nanostructuration represents a key step to control the size and the distribution of CNTs. The nanostructuration for selective growth of CNTs with a specific pattern can be made using electron beam lithography for instance. However, this technological step does not allow us to obtain large nanostructure surfaces and requires an *ex situ* process which induces a nondesired oxidation of the catalyst [11]. The *in situ* nanostructuration of catalyst film can be carried out as we will show in this study by $H_2$ plasma pre-treatment. Another catalyst nanostructuration technique was reported recently allowing us to obtain isolated nanoparticles using a copolymer [12]. The nanostructuration process we have developed in our study allow the obtaining and the control of the distribution of catalyst nanoparticles on a large surface and without any contamination. In this paper, we report mainly on the interest in using the MPACVD technique to produce isolated bundles of carbon nanotubes and on the effect of the thickness and the pre-treatment of the film catalyst on the structure and the diameter of produced CNTs. The formation of isolated bundles of CNTs opens an interesting perspective in terms of chemical functionalization efficiency, since the bundles are not aggregated. We used atomic force microscopy (AFM), scanning electron microscopy (SEM), transmission electron microscopy (TEM), and Raman spectroscopy to analyze the structure and the nature of the CNTs. AFM was used to determine the catalyst particle size in correlation with the catalyst film thickness and plasma power as well.

## 2. Experiments

In this study, we investigated in the first part the effect of the $H_2$ plasma pre-treatment microwave power (varying from 250 to 450 W) and the effect of catalyst thickness (2, 5, and 10 nm) on the diameter and density of iron catalyst nanoparticles The second part dealt with the carbon nanotubes grown in a $CH_4$–$H_2$ gas mixture after the pre-treatment step. The effect of $CH_4$ concentration was studied in relation to the catalyst nanoparticles' size. The $CH_4$ concentration was varied from 10% to 40% in the total $CH_4$–$H_2$ gas mixture. The substrates used in this study were silicon (100) covered by different Fe catalyst thicknesses, which we deposited with a high vacuum thermal deposition system. The reactor used for growing the carbon nanotubes was composed of a cylindrical quartz tube (50 mm in diameter, 350 mm in length) which intersected a rectangular waveguide, the dimensions of which were chosen to drive the TE10 mode of a 2.45 GHz microwave provided by a 0–1200 W power generator. The plasma was generated in the cylindrical tube. The temperature was measured by means of an infrared bicolor pyrometer. The gas mixture composition was ensured by mass flowmeters that were computer-controlled in order to maintain both the $CH_4$–$H_2$ ratio and the total pressure at constant values [10, 13].

## 3. Results and discussion

### *3.1. Pre-treatment*

In order to understand and to control the growth of CNTs, we studied the effect of the hydrogen plasma pre-treatment (plasma power) on our iron catalyst. Figure 1 shows SEM and AFM images of the surface of an as-deposited 10 nm Fe film thermally evaporated onto a silicon substrate. The film is continuous and has no defects.

When this 10 nm continuous iron film is subjected to a hydrogen plasma pre-treatment for 2 min under different plasma power, its surface topography changes and becomes dominated by islands of about 150 nm in diameter (figure 2). This agglomeration is driven by a surface and elastic minimization, enabled by the increase of the surface mobility of the metal atoms during the plasma pre-treatment [14]. This plasma pre-treatment is believed to create smoother and more homogeneous nanoparticles with a higher nucleation density [15, 16] compared to catalyst thermal pre-treatment. Since nucleation is dependent on the plasma parameters, we studied the effect of plasma microwave power on the nucleation of the iron catalyst. First, as microwave power was increased from 250 to 350 W, the average size of the nanoparticles decreased from 200 to 100 nm (figure 2(a)) and the catalyst density increased following the tendency. This can be attributed to the fact that the increase of plasma density induces more gas dissociation and more ion bombardment energy, which reduces the film to smaller nanoparticles. However, when the microwave power exceeds 300 W, as can be seen

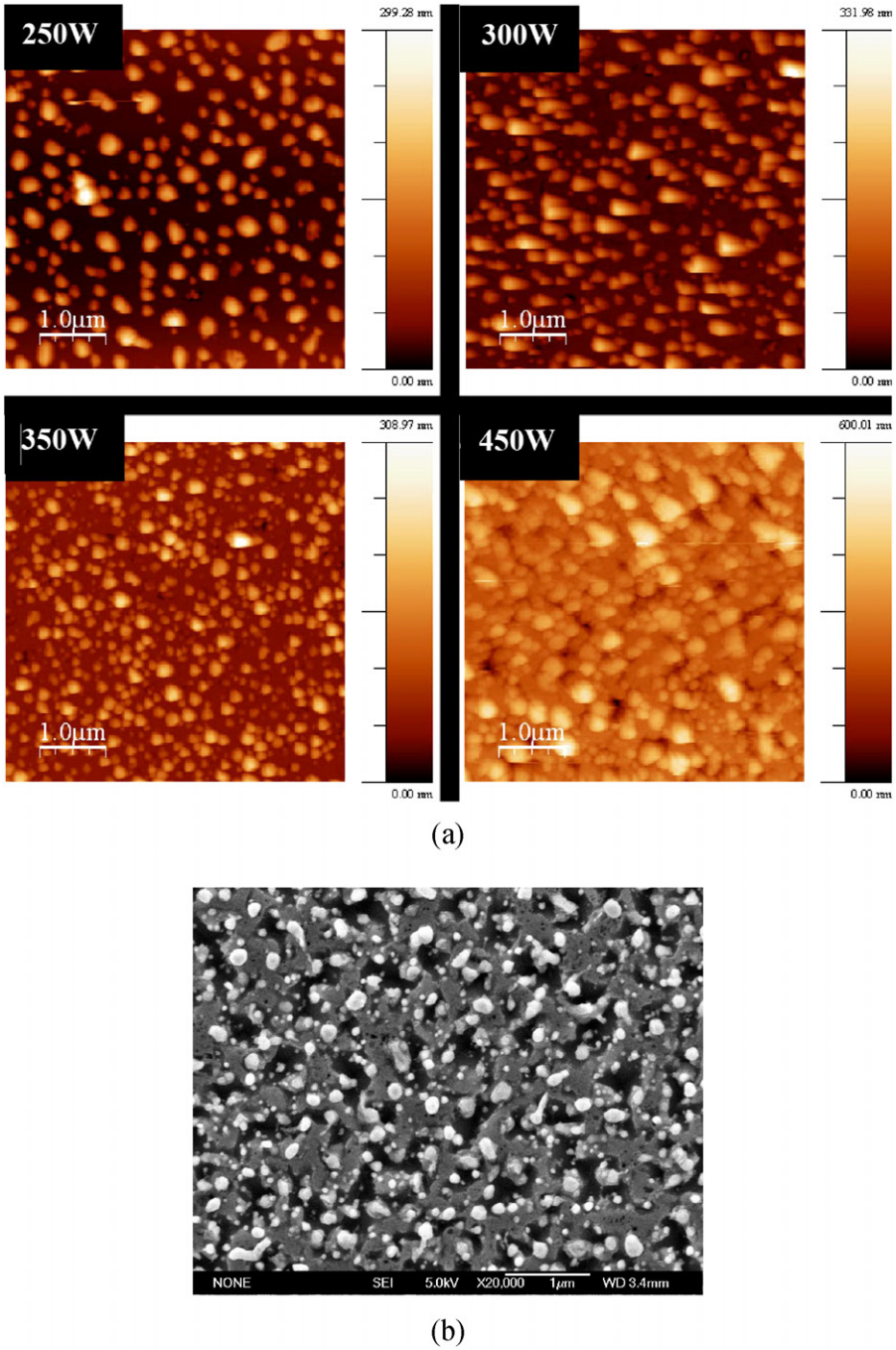


**Figure 2.** (a) AFM micrographs of pre-treated 10 nm iron catalyst film as a function of microwave power. (b) SEM micrograph showing more clearly the alteration of the catalyst surface at high microwave power.

in the AFM and SEM micrographs in figure 2, we observe an alteration in the surface, an increase in the diameter of the particles, and a reduction in the density (iron volume) compared to the previous plasma conditions. Under these conditions, the etching effect becomes dominant, and the ion bombardment is so strong that it damages the iron film and the silicon substrate (figure 2(b)). To explain the increase in the particle size, we suggest that the high surface temperature makes the iron particles conglomerate to form bigger particles.

On the other hand, the effect of the thickness of the catalyst is shown in figure 3. One can observe that the size of the Fe islands is dependent on the initial thickness of the deposited catalyst film. Under the same plasma conditions, thicker iron films (10 nm), yield larger Fe islands, with a mean diameter of about 100 nm, while thinner films (2 nm) result in smaller islands having a mean size of 10 nm. A 5 nm iron film gave a nanoparticle diameter of approximately 20 nm.

### *3.2. CNT growth*

Concerning the growth step of the CNT, we first tried to grow carbon nanotubes without an iron catalyst pre-treatment, but with no success. In our reactor, the iron catalyst needs a pre-

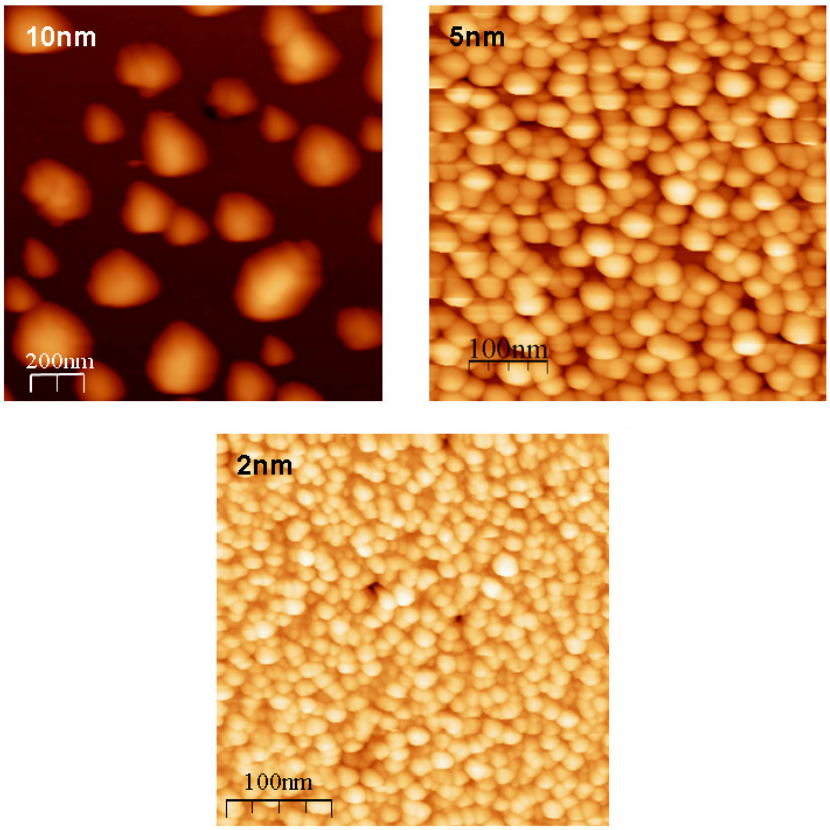


**Figure 3.** AFM micrographs of pre-treated iron catalyst as a function of catalyst thickness.

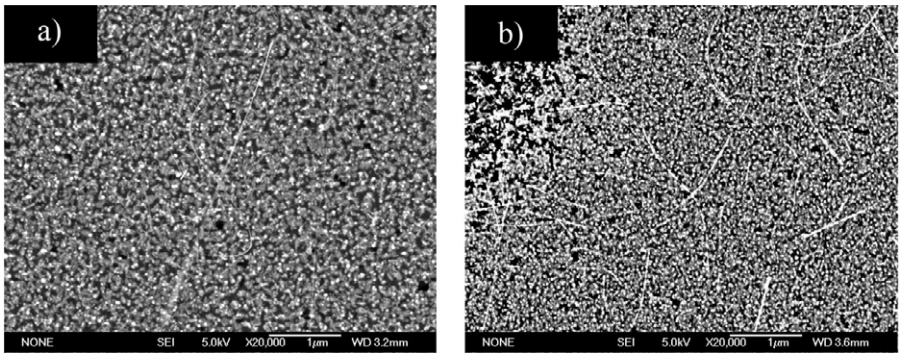


**Figure 4.** SEM micrographs illustrating the growth of CNTs on (a) 5 nm and (b) 2 nm iron catalyst film thicknesses.

treatment in order to grow carbon nanotubes. Figures 4(a) and (b) show SEM micrographs of carbon nanotubes grown by MPACVD on 2 and 5 nm thick iron catalysts. Prior to growth, the samples underwent 15 min of hydrogen plasma pre-treatment with a microwave power of 300 W. The duration of the pre-treatment was optimized before. These pre-treatment conditions were chosen to grow an acceptable quantity of CNTs. After pre-treatment, and without stopping the plasma, a $CH_4$:$H_2$ (30:70) gas mixture was introduced into the chamber and left to grow for 30 min.

For the 5 nm iron catalyst, the clusters are about 20 nm in diameter (determined by atomic force microscopy) and some CNTs can be observed on the surface. With the smaller catalyst thickness of 2 nm, the catalyst cluster size decreased to about 10 nm and the CNT density increased. According to the diffusion model [17, 18], which is widely used for interpreting CNT growth on catalyst clusters, we suggest that, for thicker catalyst films, the average size of the clusters is larger than the diffusion length of the carbon atoms. Therefore, carbon atoms cannot diffuse onto the backside of the iron nanoparticles and grow CNTs. For the 2 nm Fe film thickness, the catalyst clusters are smaller than the diffusion length, which enhances CNT growth. We note that CNTs have not grown as a dense mat, the surface density of the CNTs is weak and this can be very useful to synthesize isolated bundles of CNTs.

TEM analysis (figure 5) shows that in the case of a 2 nm thick catalyst film, MPACVD-grown CNTs consist of two or three walls and the average outer diameter is about 5 nm.

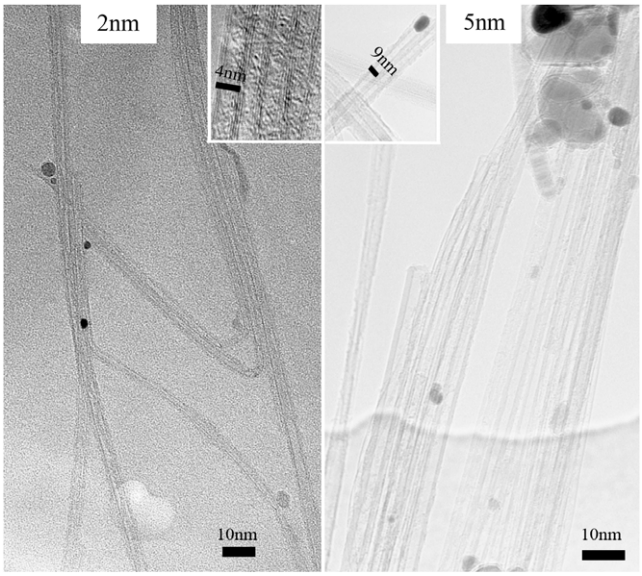


**Figure 5.** TEM micrographs of CNTs grown on 2 nm and 5 nm iron catalyst thicknesses, respectively.

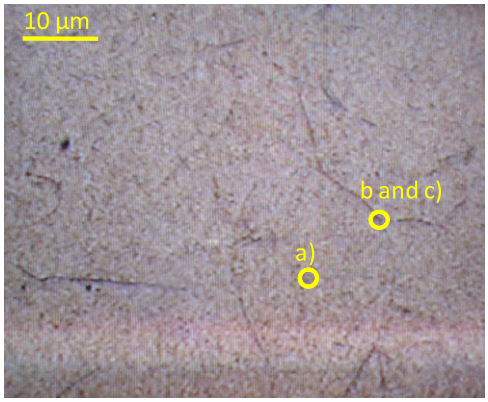


**Figure 7.** Laser spot locations on the optical microscopic image of the sample grown under 30% methane ratio on the 5 nm thick iron catalyst film for the Raman spectra (a), (b), and (c) reported in figure 8.

Statistical measurements done on TEM micrographs for two different iron thicknesses show that, as the thickness of the iron film increased from 2 to 5 nm, the average outer diameter of the CNTs was increased from 5 to 10 nm (figure 5). This can be explained by the fact that thicker Fe films result in larger catalytic nanoparticles, which consequently nucleate larger diameter CNTs since these are closely correlated to the initial catalyst island dimensions. This result agrees well with previous reports [19].

The effect of $CH_4$ concentration on CNT growth was investigated. The SEM micrographs shown in figure 6 reveal that the density of the CNTs increases as the ratio of methane is incrementally increased from 10 to 30% using a 5 nm thick catalyst film. A further increase in the methane inlet composition resulted in no observable CNTs. The same tendency was observed on 2 nm thick catalyst film. The decline of CNTs as the catalyst grows is due to catalyst poisoning, a phenomenon which is caused by the formation of amorphous carbon deposited on the catalyst's surface since there is more carbon contribution at higher methane ratios.

The CNTs' density is also dependent on pre-treatment time: when passing from 15 to 2 min of pre-treatment, CNT density decreased. We noticed that the decrease was greater with 2 nm Fe film [11]. TEM micrographs (not shown here) showed that the CNT outer diameter increased with the increase of $CH_4/H_2$ ratio.

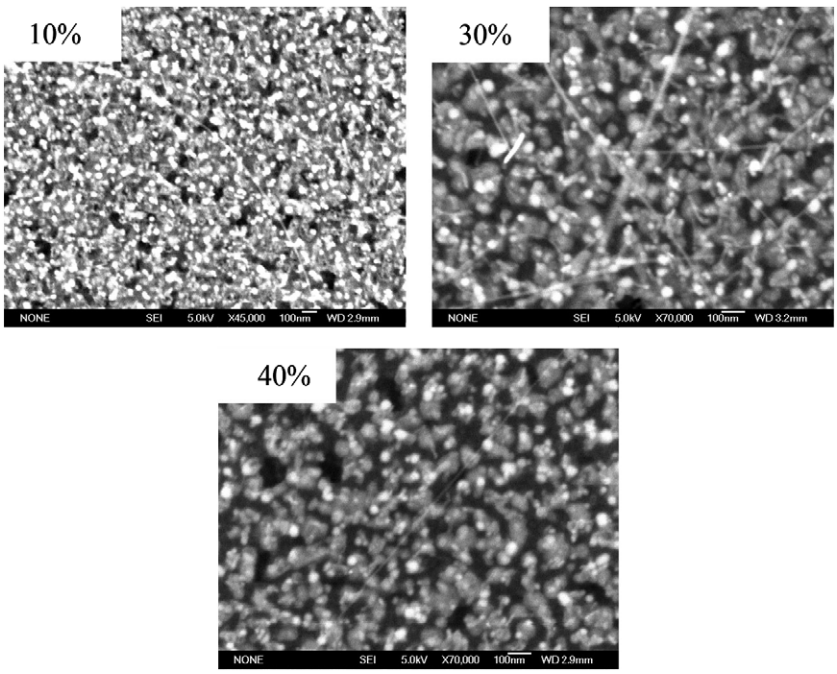


**Figure 6.** SEM images of CNTs grown under different methane ratios for a 5 nm thick iron catalyst film.

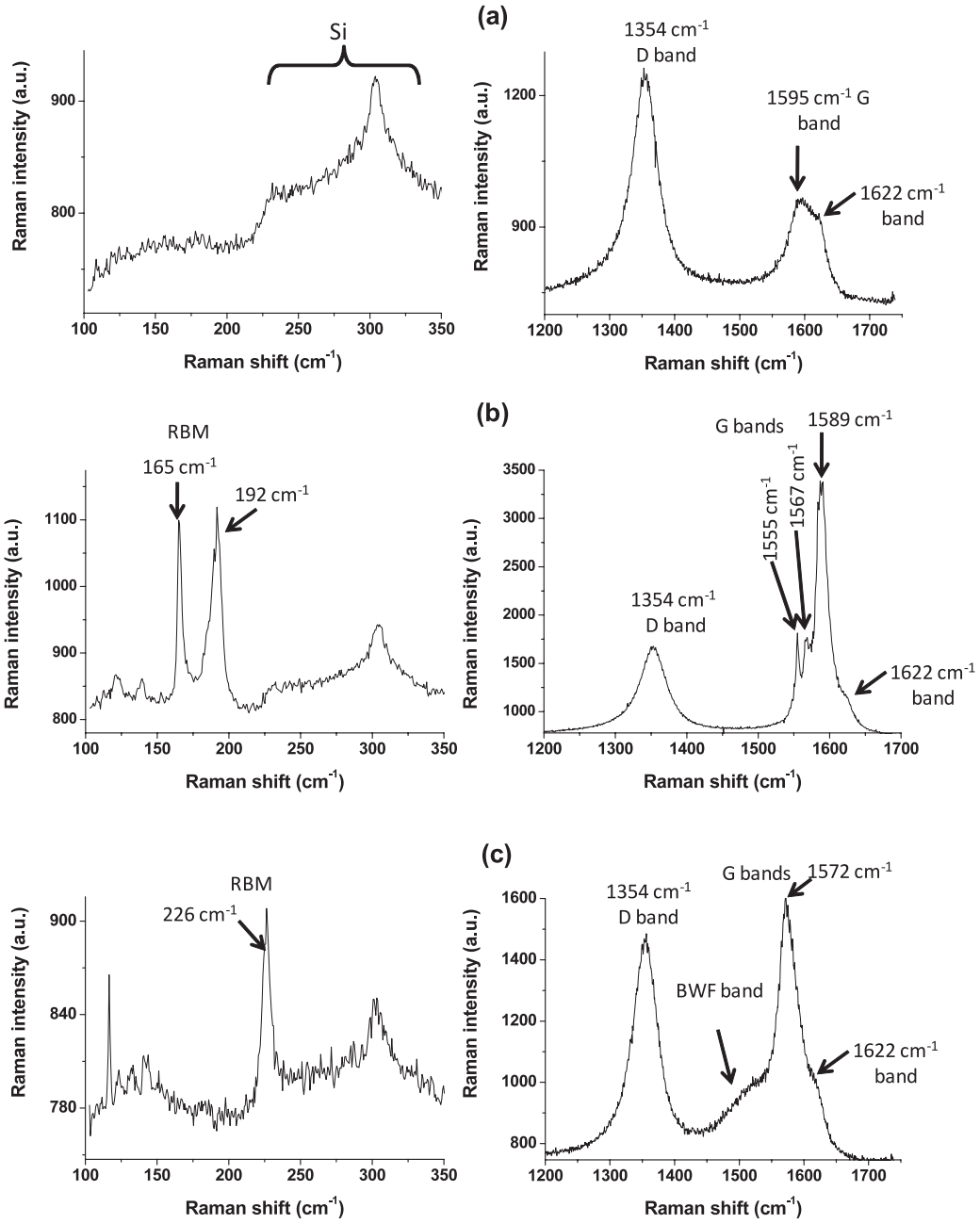


**Figure 8.** Raman spectra of the sample grown under 30% methane ratio on the 5 nm thick iron catalyst film. (a) Spectrum of an area with no CNT bundle, (b) and (c) Raman response of a bundle of CNTs at two different laser irradiances ((b): 2 kW cm$^{-2}$; (c): 10 kW cm$^{-2}$).

Raman spectroscopy measurements were done on our samples in order to investigate crystallization and defects in CNTs grown by MPACVD. An argon laser excitation wavelength of 514 nm was used on samples of different methane ratios (20%, 30%, and 40% of $CH_4$). Figure 8 shows the Raman spectra of the sample synthesized using 30% of $CH_4$. Figure 8(a) exhibits the typical spectrum carried out in an area of the sample for which no bundle of CNTs was optically visible under the microscope objective (see figure 7), while figures 8(b) and (c) show the response when the Raman beam was directly focused on a visible bundle of CNTs. In the case of figure 8(c), the laser irradiance was increased slightly (from 2 to 10 kW cm$^{-2}$) to produce a laser heating effect of the sample. This heating effect was beneficial to change the resonance conditions of the tubes [20]. As expected, Raman spectra in figure 8(c) are different from the ones of figure 8(b), while the analysis was done at the same location on the sample (figure 7). One should note that the laser power was chosen to assure a reversible heating effect, and not an irreversible burning of CNTs. This was checked by decreasing the laser power back to its initial value and verifying that the spectra were similar to the ones of figure 8(b). When no bundles of CNTs are visible (figure 8(a)), strong silicon, disordered carbon (D line), and crystallized carbon (G line) peaks are

recorded, which corresponds to a layer of amorphous and crystalline carbonaceous structures. By contrast, clear radial breathing modes (RBM) are detected in figure 8(b) at 165 and 192 $cm^{-1}$. These RBM modes certainly come from the double-walled CNTs present in the sample [21]. Using the simple relationship between tube diameter $d$ and RBM wavenumber $\omega$ indicated in equation (1) [22], the corresponding diameters of the CNTs are respectively 1.38 and 1.18 nm. These values certainly account for RBM modes of the inner tubes of double-walled CNTs if one compares them to the average diameter of tubes obtained by TEM analysis.

$$\omega(\mathrm{cm}^{-1}) = \frac{227}{d(\mathrm{nm})}. \quad (1)$$

The ratio $I_D/I_G$ between G-band intensity around 1500–1600 $cm^{-1}$ and D-band intensity around 1350 $cm^{-1}$ cannot be used in our case to estimate the number of defects of the investigated CNTs. Indeed, these bands also contain some contribution of the carbonaceous structures lying close to the CNTs bundles. The spot size of our laser has a diameter of $\sim$1 $\mu$m using our 100$\times$ objective, which signifies that figure 8(b) is the sum of a spectral contribution of the investigated CNT bundle and the same kind of spectral contribution of carbonaceous structures reported in figure 8(a). However, the clear RBM signature and the high increase of the G-band intensity near 1555, 1567, and 1589 $cm^{-1}$, with almost no increase of the D-band intensity if compared to figure 8(a), prompt us to think that the produced CNTs have quite good quality with very few defects. This is consistent with the good structural quality observed in figure 5 by TEM. Interestingly, the G-bands of figure 8(b) are characteristic of semiconducting CNTs. When laser heating is applied at the same location, the resonance window shifts and metallic CNTs become resonant, as shown by the Bret–Wigner–Fano (BWF) shoulder indicated in figure 8(c) [22]. This experiment evidences that both metallic and semiconducting tubes are present in our isolated bundles. For 20% $CH_4$, the Raman spectrum shows a very weak RBM peak, and no RBM signal was obtained for the sample made with 40% of $CH_4$ (spectra not showed). In regard to these results we can conclude that, in our study, when the methane ratio is increased over 30%, more carbonaceous structures are deposited to the detriment of CNTs. An abundance of carbon atoms is not beneficial for growing clean carbon nanotubes.

## 4. Conclusion

In this work we have studied the effect of hydrogen plasma pre-treatment microwave power on the clustering of an iron catalyst layer and the effect of pre-treatment for three different thicknesses (2, 5, and 10 nm). We have found that the nanoparticle size is controlled by microwave plasma power and by the thickness of the catalyst film. Concerning CNT growth, we have found a relationship between the nanoparticle size and the CNT diameters. As the thickness of the iron film increased, the average diameter of the CNTs increased. We found that the concentration of $CH_4$ has an effect on the density of the produced CNTs. TEM micrographs indicated that the diameter and the nature of the CNTs can be controlled by hydrogen plasma pre-treatment, $CH_4$ concentration, and the thickness of the catalyst film. Raman characterization showed that the obtained CNTs are of a good quality and that the isolated bundles contain both semiconducting and metallic tubes.

## Acknowledgments

The authors would like to thank Dr Brigitte Vigolo for fruitful discussions and Dr Jaafar Ghanbaja for TEM analyses.

## References

[1] Melechko A V, Merkulov V I, McKnight T E, Guillorn M A, KleinK L, Lowndes D H and Simpson M L 2005 *J. Appl. Phys.* **97** 041301
[2] Martel R, Schmidt T, Shea H R, Hertel T and Avouris P 1998 *Appl. Phys. Lett.* **73** 2447
[3] Gröning P, Ruffieux P, Schlapbach L and Gröning O 2003 *Adv. Eng. Mater.* **5** 541
[4] Wang J 2005 *Electroanalysis* **17** 7
[5] Cantalini C, Valentini L, Lozzi L, Armentano I, Kenny J M and Santucci S 2003 *Sensors Actuators* B **93** 333
[6] Meyappan M, Delzeit L, Cassel A and Hash D 2003 *Plasma Sources Sci. Technol.* **12** 205
[7] Minea T M, Point S, Granier A and Touzeau M 2004 *Appl. Phys. Lett.* **85** 1244
[8] De Poucques L, Bougdira J, Hugon R, Henrion G and Alnot P 2001 *J. Phys. D: Appl. Phys.* **34** 896
[9] Rizk S, Assouar M B, Gatel C, Belmahi M, Lambert J and Bougdira J 2008 *Diamond Relat. Mater.* **17** 1660
[10] Lamara T, Belmahi M, Henrion G, Hugon R, Bougdira J, Rémy M and Fabry M 2005 *Surf. Coat. Technol.* **200** 1110
[11] Rizk S, Assouar M B, De Poucques L, Alnot P and Bougdira J 2009 *J. Phys. Chem.* C **113** 8718
[12] Wang P, Lu J and Zhou O 2008 *Nanotechnology* **19** 185605
[13] Chatei H, Belmahi M, Assouar M B, Le Brizoual L, Bourson P and Bougdira J 2006 *Diamond Relat. Mater.* **15** 1041
[14] Jiran E and Thompson C V 1990 *J. Electron. Mater.* **19** 1153
[15] Wang S, Wang P and Zhou O 2006 *Diamond Relat. Mater.* **15** 361
[16] Hoffmann S, Ducati C, Robertson J and Kleinsorge B 2003 *Appl. Phys. Lett.* **83** 135
[17] Baker R T K 1989 *Carbon* **27** 315
[18] Rodriguez N M 1993 *J. Metter. Res.* **80** 3233
[19] Wei Y Y, Eres G, Merkulov V I and Lowndes D H 2001 *Appl. Phys. Lett.* **78** 1394
[20] Olevik D, Soldatov A V, Dossot M, Vigolo B, Humbert B and McRae E 2008 *Phys. Status Solidi* b **245** 2212
[21] Liu B C, Yu B and Zhang M X 2005 *Chem. Phys. Lett.* **407** 232
[22] Jorio A *et al* 2002 *Phys. Rev.* B **66** 115411